Visible Light Communications: Filter-less Wavelength Division Multiplexing

Paul Anthony Haigh
Intelligent Sensing and Communications Group
Newcastle University
Newcastle upon Tyne, NE1 7RU, UK
paul.haigh@newcastle.ac.uk

Andrew Burton
ISOCOM Ltd.
Peterlee, SR8 2RR, UK
aburton@isocom.uk.com

Petr Chvojka
Faculty of Electrical Engineering
Czech Technical University in Prague
Prague 16627, Czech Republic
petr.chvojka@fel.cvut.cz

Stanislav Zvanovec
Faculty of Electrical Engineering
Czech Technical University in Prague
Prague 16627, Czech Republic
xzvanove@fel.cvut.cz

Zabih Ghassemlooy
Optical Communications Research Group
Northumbria University
Newcastle upon Tyne, NE1 8ST, UK
z.ghassemlooy@northumbria.ac.uk

Izzat Darwazeh
Communications and Information Systems Group
University College London
London, WC1E 6BT, UK
i.darwazeh@ucl.ac.uk

***Abstract*—In this paper, we propose a new receiver and demodulation method for use in wavelength division multiplexed visible light communications systems, utilising the natural diversity offered by photodiodes. This is based on the wavelength dependent photodiode responsivities, which lead to different signal-to-noise ratios at the receiver. Using this method, it is possible to transmit independent information using on different wavelengths but where signals occupy the same electrical frequency range and where they would, otherwise, interfere. We illustrate and experimentally demonstrate that through simple subtractions the signals can be extracted with the constellations showing *Q*-factors corresponding to sufficiently low bit error rates.**

***Index Terms*—Digital signal processing, non-orthogonal, optical communications, visible light communications, wavelength division multiplexing**

I. Introduction

Achieving high data rates is a key challenge in visible light communication (VLC) systems. A limitation on the bandwidth is mainly introduced by the light-emitting diodes (LEDs) that are commonly used as the transmitter, which reduces the raw modulation bandwidth to a few MHz [1], [2]. At present, Gb/s transmission speeds have been achieved that utilise four key methods including (*i*) bandwidth expansion by circuit designs, which uses circuit elements to equalise the capacitive behaviour of the LEDs [3] and photodetectors [4]; (*ii*) advanced modulations, which are used to maximise the number of bits/symbol that can be transmitted on a single wavelength [5]; (*iii*) digital signal processing (DSP), i.e. post-equalisation, which removes inter-symbol interference (ISI) by using intelligent filter designs [6]; and (*iv*) wavelength-division multiplexing (WDM), which combines the previous three methods and re-uses them to drive different wavelengths and provide additional spectrum.

The main disadvantage of WDM is the fact that it requires independent dichroic filters, photodetectors and receiver circuits for each wavelength used [7]. However, this is neither practical nor cost-effective. Recently, non-orthogonal modulation techniques such as spectrally efficiency frequency division multiplexing (SEFDM) [8], super-Nyquist carrierless amplitude and phase (CAP) modulation [9] and faster-than-Nyquist (FTN) [10] have been investigated in VLC systems. These modulation formats are designed to improve the capacity of a communications link through purposely introducing inter-carrier interference or ISI for SEFDM and FTN, respectively. They operate on the premise of overlapping energy, hence violating the Nyquist criterion to increase spectral efficiency (and therefore data rate) at the cost of increased bit-error rate (BER) or computational complexity at the receiver [8]–[10]. Recent work has demonstrated that totally overlapped signals in the frequency domain can be recovered successfully using DSP methods [11], provided there is diversity between the signals such as variations in amplitude.

In this paper, we propose to transmit independent signals on two different wavelengths and detect them using a single photodetector-based receiver circuit prior to separation using self-interference cancellation (SIC) [12] as a proof-of-concept. Note that in the proposed system, no additional op-

This work is supported by the UK EPSRC grant EP/P006280/1: MARVEL, CTU Prague and KU Leuven (CELSA) project "Polarization In wireless CommuNICations (PICNIC)" and by the European Union's Horizon 2020 research and innovation programme under the Marie Sklodowska-Curie grant agreement no 764461 (VISION).

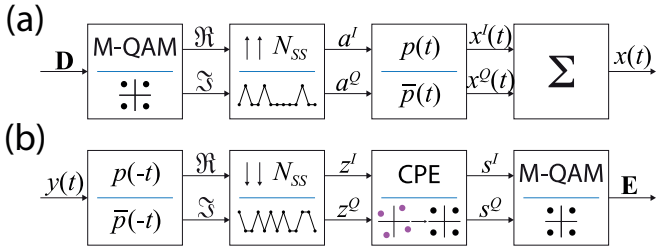

Fig. 1. CAP: (a) modulator, and (b) demodulator.

tical wavelength filters are employed as in previous literature [7]. We postulate that through the natural inequivalence of the optical power output of different coloured LEDs, and the variability of the responsivity versus wavelength of silicon detectors, sufficient diversity is introduced between signals to enable signal recovery with improved data rates.

The rest of the paper is organised as follows. Section II outlines the proposed filters-less WDM experimental testbed. The results are presented in Section III and finally, the conclusion is given in Section IV.

II. PROPOSED FILTER-LESS WDM TEST SETUP

The proposed system is modulation format independent, however we have elected to use CAP modulation due to its popularity in the literature [6], [7], [9], [11]. The modulator for the CAP system is illustrated in Fig. 1(a).

A stream of data symbols $\mathbf{D}$ is mapped onto the M-ary quadrature amplitude modulation (M-QAM) constellation, where $k = log_2 M$ and k is the number of bits/symbol. The real ($\Re$) and imaginary ($\Im$) components are then separated and up-sampled via zero-padding at a rate of N_{ss} before pulse shaping. The basis function of the pulse shape is generally a square root-raised cosine (RRC), however there are advantages when it is replaced by other parametrically designed filters as reported in the literature [13]. The basis function is then multiplied with the cosine ($\Re$) and sine ($\Im$) waves operating at the carrier frequency f_c, in order to generate the final pulse shaping filters $p(t)$ and $\overline{p}(t)$, the theory of which have been extensively reported in the literature [13]. The real and quadrature signals are then summed to generate $x(t)$ for transmission.

The demodulation of CAP signals is simply the reverse process, see Fig. 1(b). The received signal is the noise-corrupted received signal $y(t) = x(t) * y(t) + n(t)$, where $h(t)$ is the channel impulse response, $n(t)$ is the additive white Gaussian noise and $*$ indicates time-domain convolution. It is passed through time-reversed matched filters before down-sampling at a rate of N_{ss}. Common phase error (CPE) correction is then performed via a blind method [14] before de-mapping of the M-QAM constellation and estimation of the transmitted bit vector $\mathbf{E}$.

In the proposed system, we have used two wavelengths of 452 nm (λ_B, blue) and 637 nm (λ_R, red), which were selected due to their spectral orthogonality in order to reduce crosstalk. The normalised emission spectra of the LEDs are illustrated in Fig. 2, along with the responsivity of the OSD15-5T silicon photodiode. It should be noted that both LEDs are contained

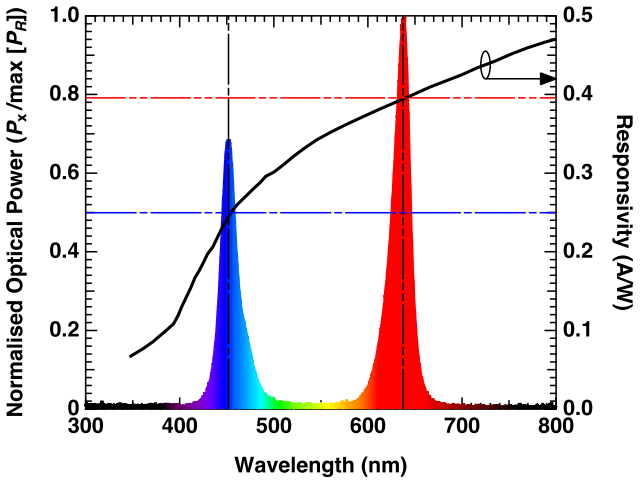

Fig. 2. Emission spectrum of the LEDs normalised to the maximum of the red emitter (left axis) and responsivity of the Centronics OSD15-5T silicon photodiode (right axis).

within a single off-the-shelf red, green and blue (RGB) chip. However, the green chip remains unused and in the off-state throughout the measurement to avoid possible saturation of the front end. It is clear that both LEDs used have (a) different optical power outputs for the same drive current I_d of 350 mA and (b) different responsivities for different wavelengths of the photodetector. It is our hypothesis that these inequalities will provide sufficient diversity to employ SIC techniques at the receiver and therefore support simultaneous independent parallel data transmission.

The overall simplified system block diagram is shown in Fig. 3. Initially, pilots are transmitted on each wavelength during an assigned unique time slot, i.e., the R system is activated while the B remains off and vice-versa. The pilots consisting of 1,000 symbols are broadcast in order to obtain the amplitude and phase information required at the receiver, which is later used to reconstruct the transmitted symbols. Following pilot transmission, two independent pseudorandom binary sequences $\mathbf{D}_R$ and $\mathbf{D}_B$, both of length $2^{15} - 1$, are generated for λ_R and λ_B, respectively. The modulated sequences of the two signals $x_R(t)$ and $x_B(t)$ are then used for intensity modulation of two LED chips via custom-designed driving circuits and a Keysight M8190A arbitrary waveform generator. The *L-I-V* characteristics and bandwidth

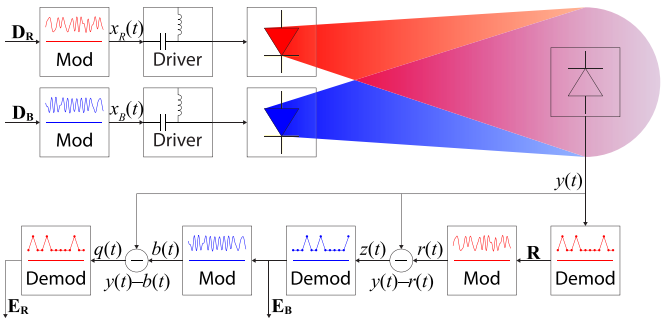

Fig. 3. Simplified experimental test setup.

of the LEDs under test can be found in the literature [15].

The modulated light beam is transmitted over a free space link of 0.5 m and is detected by a Centronics OSD15-5T silicon photodiode, which is ac coupled to a transimpedance amplifier (Analog Devices AD8015) with a gain of 10 kΩ. The signals are captured using a Keysight DSO80604B real-time oscilloscope.

The received signal is given by:

$$y(t) = h(0) \cdot [\gamma(\lambda_B) P_B x_B(t) + \gamma(\lambda_R) P_R x_R(t)] + n(t) \quad (1)$$

where $h(0)$ is the line of sight channel impulse response modelled here as a frequency and wavelength independent channel with gain < 1 and is assumed equal for both LEDs due to the fact they have approximately equal path lengths. The responsivity of the photodetector $\gamma(\lambda)$ is 0.25 and 0.39 A/W at λ_B and λ_R, respectively, and P is the transmit optical power.

Next, the signal is demodulated with respect to the strongest wavelength first, i.e., the R component since it has a higher transmitted power and corresponds to a region of greater responsivity in silicon, and therefore results in a stronger received signal. Hence, the output of the first demodulation stage is given as $\mathbf{R}$, i.e. the estimated transmit vector of the bits transmitted on the R LED. An example of the received constellation before QAM de-mapping is illustrated in Fig. 4, where the received symbols can be classified in two different ways. Firstly, the symbols carried on the R wavelength are shown in the four main Gray-coded quadrants, which can be demodulated using the standard method of hard threshold detection using the red dashed line. Secondly, inset in each quadrant, are the symbols transmitted via the B LED superposed onto the R symbols. They can be estimated through threshold detection using the blue dashed line (illustrated in upper right quadrant only) but first the red-wavelength symbols must be subtracted. Thus, following detection and hard decision to obtain $\mathbf{R}$, the recovered bits are re-modulated back to the ideal constellation and scaled according to the amplitude information recovered through the pilot signal. Following re-modulation and rescaling, an ideal version of the re-modulated (estimated) signal $r(t)$ is subtracted from the received signal $y(t)$, we have:

$$z(t) = y(t) - r(t) \quad (2)$$

where $z(t)$ is an estimate of the blue component of the signal.

The same demodulation process using the same matched filters are performed, since the two signals carried on each wavelength occupy the same frequency range. Hence, the blue bit vector $\mathbf{E}_B$ uncorrupted by the R symbols can be recovered. Following this, the method is repeated for the R symbols to obtain $\mathbf{E}_R$. Both $\mathbf{E}_B$ and $\mathbf{E}_R$ are used to determine the BER. Clearly, the performance of the proposed system is heavily dependent on the received signal-to-noise ratio (SNR). To gain insight into the detailed performance of the system, we initially fixed the red LED's peak-to-peak amplitude to 750 mV_{pp}, (the M8190A maximum voltage V_{max}). The B amplitude is then varied over the range of [0.2, 0.4, 0.6, 0.8, 1]$\cdot V_{\text{max}}$. After which, the output of the R LED is reduced by 20% of V_{max} and the tests are repeated again. We also repeated this for a $k = 2$.

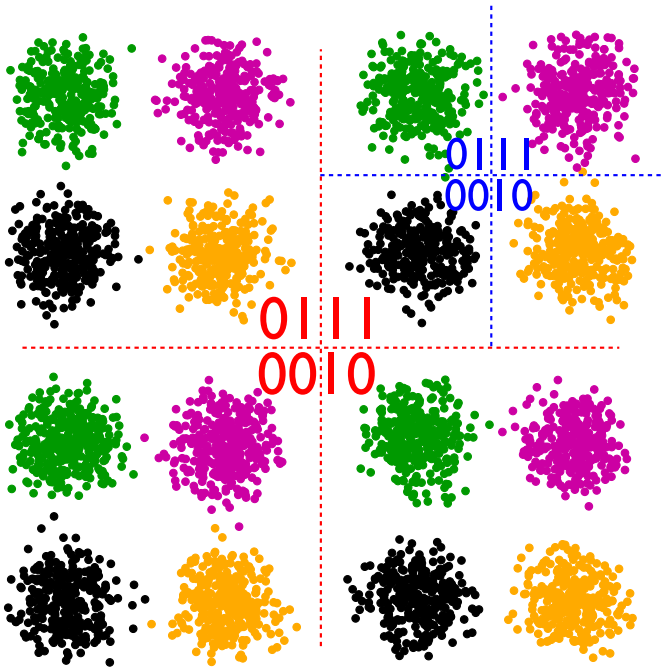

Fig. 4. Example of the received constellation; the data is first detected based on the dominant wavelength (dashed threshold), then the remaining one (dashed-dot).

III. Results

The Q-factor is measured using the relation shown in [16] and is illustrated in Figs. 5(a) and (b) for λ_R and λ_B, respectively. The first observation is that there is no performance dependence on the roll-off factor (refer to [17]), as indicated by the solid ($\beta = 0.1$) and dashed ($\beta = 0.5$) lines for both wavelengths. For both plots, the x-axis represents the variation in the V_{pp} of the signal driving the B LED as a percentage of V_{max}. The solid horizontal black line indicates a Q-factor of 8.5 dB, which approximately corresponds to a BER of $3.8 \cdot 10^{-3}$ (i.e., the 7% forward error correction (FEC) limit). The green region above the FEC limit is where successful data transmission can be supported. Clearly, from the simultaneous inspection of Figs. 5(a) and (b), for ac voltage swings of $V_{\text{B}} = V_{\text{R}}$, satisfactory Q-factors can be supported with both wavelengths.

The reason being the nonlinear characteristics of the photodetector responsivity versus wavelength ensures that the difference in received signal amplitudes between the two data streams is sufficient to allow their independent demodulation. For $V_{\text{B}} > V_{\text{R}}$, we observe a significant Q-factor penalty and therefore both systems fail. Note, this penalty is because of the amplitudes for each system become approximately equal, thus introducing errors in the initial red-demodulation stage, resulting in an inaccurate estimation of $\mathbf{R}$ (see Fig. 3). Thus, the blue-data is also inaccurately estimated due to the error propagation. However, for removing the inter-wavelength interference there are more computationally complex methods including the use of artificial neural networks [18]. For $V_{\text{B}} >> V_{\text{R}}$, the B channel also suffers from a significantly higher Q-factor penalty. This is because the measured noise power becomes approximately equivalent to the distance of

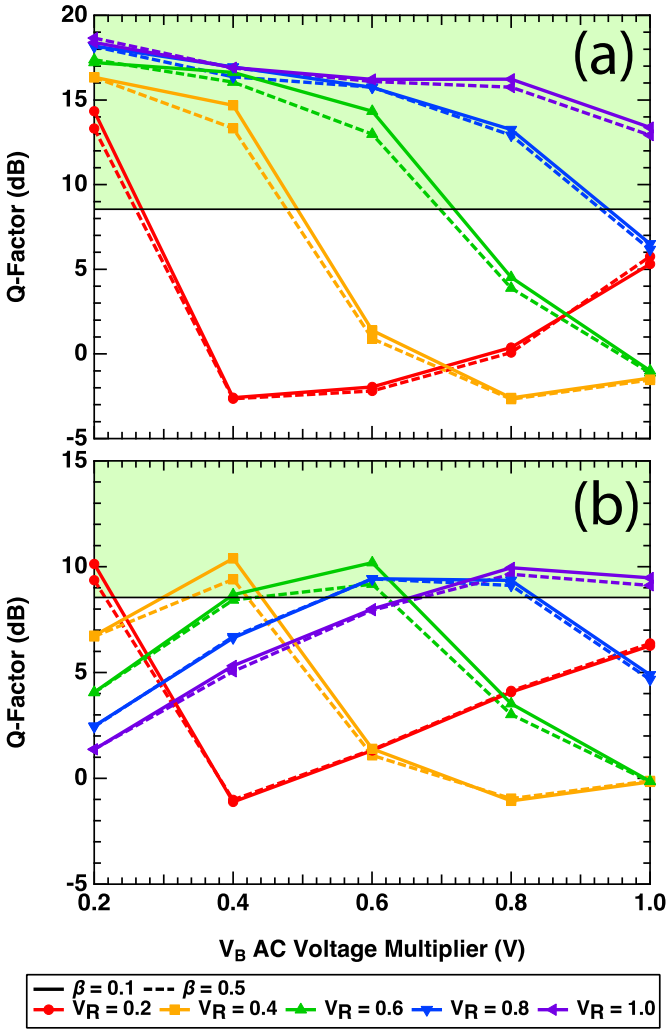

Fig. 5. The Q-factor performance of: (a) R and (b) B LEDs as a function of ac voltage and excess bandwidth factor. Note, green area indicates sufficiently low BER.

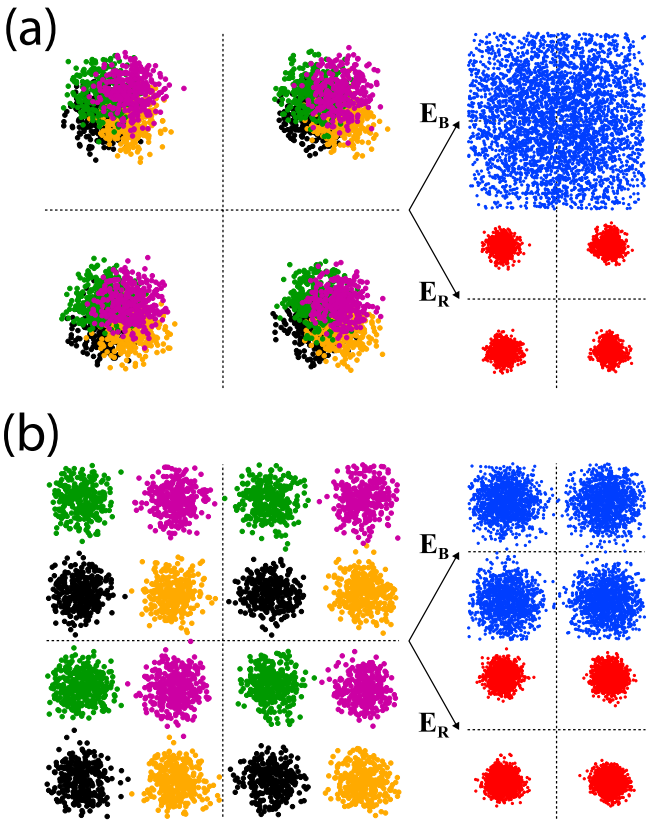

Fig. 6. Recovered constellations of: (a) $V_{\mathrm{R}} = V_{\max}$ (successful), $V_{\mathrm{B}} = 0.2V_{\max}$ (failure) and (b) $V_{\mathrm{R}} = V_{\max}$ (successful), $V_{\mathrm{B}} = 0.8V_{\max}$ (successful).

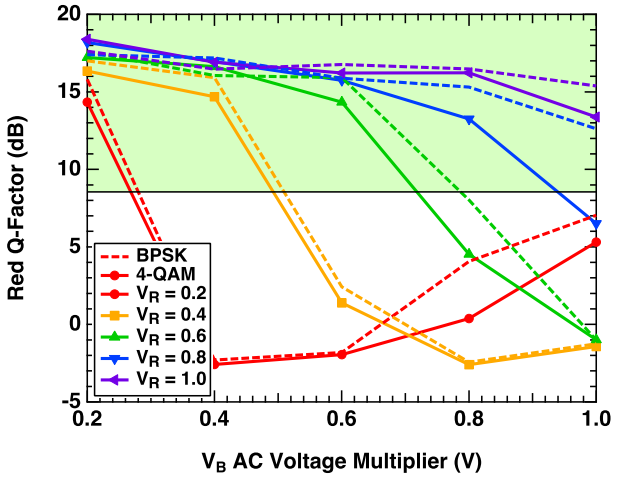

Fig. 7. 4-QAM Q-factor performance of the R LED .

the constellation points of the B channel. Hence, the B constellation cannot be recovered via hard threshold detection due to significant overlap of the constellation points. This concept is best illustrated in Figs. 6(a) for a failure ($V_{\mathrm{R}} = 1$, $V_{\mathrm{B}} = 0.2$) and (b) successful ($V_{\mathrm{R}} = 1$, $V_{\mathrm{R}} = 0.8$) case.

For binary phase shift keying (BPSK) based VLC link, the Q-factor for the R LED follows almost the same performance trend as that of 4-QAM, refer to Fig. 7. Note, the Q-factor for BPSK is marginally higher than 4-QAM. This is because of fewer interfering symbols in BPSK. These results demonstrate that the proposed technique is independent of modulation format, which is a desirable feature to have.

The symbol rate transmitted, considering the 5 MHz signal bandwidth carried on each wavelength was $\sim$ 4.5 Msym/s thus resulting in gross transmission rates of $\sim$ 18 Mb/s and $\sim$ 9 Mb/s for 4-QAM and BPSK, respectively. Note that, this is before overhead removal, thus giving an aggregate improvement of 100%, which is a result of the additional wavelength used for transmission in the same frequency range. Incidentally, more wavelengths could be used that further (linearly) improve the transmission speed in the same space. However, this would be at the cost of increased SNR requirement and cross-talk between wavelengths would become more critical.

IV. Conslusion

This work demonstrates a technique for data recovery in a wavelength-multiplexed-based VLC link, where there is no requirement for neither receiver optical filters nor detection matrix inversion. We showed that through the use of the

natural diversity introduced by the wavelength dependent responsivity of the photodiode, information carried on two modulated VLC-LEDs, operating at different wavelengths, can be separated and demodulated at the receiver with sufficiently high Q-factors (i.e., lower BERs).

REFERENCES

[1] N. Anous, M. Abdallah, K. Qaraqe, and D. Khalil, "Enhancement of Modulation Bandwidth in Wide-Angle VLC Systems via Response-Flattening Filters," in *2018 IEEE Global Communications Conference (GLOBECOM)*, Abu Dabi, 2018, pp. 1–6.

[2] Z. Ghassemlooy, W. Popoola, and S. Rajbhandari, *Optical Wireless Communications: System and Channel Modelling with MATLAB®, Second Edition*. Boca Raton: CRC Press, 2019.

[3] T. Odedeyi, P. A. Haigh, and I. Darwazeh, "Transmission Line Synthesis Approach to Extending the Bandwidth of LEDs for Visible Light Communication," in *2018 11th International Symposium on Communication Systems, Networks & Digital Signal Processing (CSNDSP)*, Budapest, 2018, pp. 1–4.

[4] A. Kassem and I. Darwazeh, "A High Bandwidth Modified Regulated Cascode TIA for High Capacitance Photodiodes in VLC," in *2019 IEEE International Symposium on Circuits and Systems (ISCAS)*, Sapporo, 2019, pp. 1–5.

[5] X. Huang, S. Chen, Z. Wang, J. Shi, Y. Wang, J. Xiao, and N. Chi, "2.0-Gb/s Visible Light Link Based on Adaptive Bit Allocation OFDM of a Single Phosphorescent White LED," *IEEE Photonics Journal*, vol. 7, no. 5, pp. 1–8, 2015.

[6] S. Liang, L. Qiao, X. Lu, and N. Chi, "Enhanced performance of a multiband super-Nyquist CAP16 VLC system employing a joint MIMO equalizer," *Optics Express*, vol. 26, no. 12, pp. 15 718–15 725, 2018.

[7] Y. Wang, L. Tao, X. Huang, J. Shi, and N. Chi, "8-Gb/s RGBY LED-Based WDM VLC System Employing High-Order CAP Modulation and Hybrid Post Equalizer," *IEEE Photonics Journal*, vol. 7, no. 6, pp. 1–7, 2015.

[8] I. Darwazeh, H. Ghannam, and T. Xu, "The First 15 Years of SEFDM: A Brief Survey," in *2018 11th International Symposium on Communication Systems, Networks Digital Signal Processing (CSNDSP)*, Budapest, 2018, pp. 1–7.

[9] P. A. Haigh, P. Chvojka, Z. Ghassemlooy, S. Zvanovec, and I. Darwazeh, "Visible Light Communications: Multi-band Super-Nyquist CAP Modulation," *Optics Express*, 2019.

[10] J. Zhou, Q. Wang, J. Wei, Q. Cheng, T. Zhang, Z. Yang, A. Yang, Y. Lu, and Y. Qiao, "Faster-Than-Nyquist Non-Orthogonal Frequency-Division Multiplexing for Visible Light Communications," *IEEE Access*, vol. 6, pp. 17 933–17 941, 2018.

[11] J. A. Altabas, S. Rommel, R. Puerta, D. Izquierdo, J. I. Garces, J. A. Lazaro, J. J. V. Olmos, and I. T. Monroy, "Nonorthogonal Multiple Access and Carrierless Amplitude Phase Modulation for Flexible Multiuser Provisioning in 5G Mobile Networks," *Journal of Lightwave Technology*, vol. 35, no. 24, pp. 5456–5463, 2017.

[12] S. Hong, J. Brand, J. I. Choi, M. Jain, J. Mehlman, S. Katti, and P. Levis, "Applications of self-interference cancellation in 5G and beyond," *IEEE Communications Magazine*, vol. 52, no. 2, pp. 114–121, 2014.

[13] P. Haigh, P. Chvojka, S. Zvánovec, Z. Ghassemlooy, and I. Darwazeh, "Analysis of Nyquist Pulse Shapes for Carrierless Amplitude and Phase Modulation in Visible Light Communications," *Journal of Lightwave Technology*, vol. 36, no. 20, 2018.

[14] S. T. Le, P. A. Haigh, A. D. Ellis, and S. K. Turitsyn, "Blind Phase Noise Estimation for CO-OFDM Transmissions," *Journal of Lightwave Technology*, vol. 34, no. 2, pp. 745–753, 2016.

[15] A. Burton, S. Zvanovec, Z. Ghassemlooy, P. A. Haigh, I. Darwazeh, and H. L. Minh, "Investigation of WDM VLC Using Standard 5 mm RGB LEDs," in *2018 11th International Symposium on Communication Systems, Networks Digital Signal Processing (CSNDSP)*, Budapest, 2018, pp. 1–6.

[16] S. Rajbhandari, P. A. Haigh, Z. Ghassemlooy, and W. Popoola, "Wavelet-Neural Network VLC Receiver in the Presence of Artificial Light Interference," *IEEE Photonics Technology Letters*, vol. 25, no. 15, pp. 1424–1427, 2013.

[17] P. Chvojka, K. Werfli, S. Zvanovec, P. Haigh, V. Vacek, P. Dvorak, P. Pesek, and Z. Ghassemlooy, "On the m-CAP Performance with Different Pulse Shaping Filters Parameters for Visible Light Communications," *IEEE Photonics Journal*, vol. 9, no. 5, pp. 1–12, 2017.

[18] Y. Ha, W. Niu, and N. Chi, "Frequency reshaping and compensation scheme based on deep neural network for a FTN CAP 9QAM signal in visible light communication system," in *17th International Conference on Optical Communications and Networks (ICOCN2018)*, vol. 11048, Zhuhai, 2019, pp. 468–474.